Jour. Fac. Sci., Hokkaido Univ., Ser. VII (Geophysics), Vol. 8, No. 1, 37-63, 1986.

Accurate Determination of Source Depths and Focal Mechanisms of Shallow Earthquakes Occurring at the Junction between the Kurile and the Japan Trenches

Jun'ichi Miyamura* and Tsutomu Sasatani

Department of Geophysics, Faculty of Science, Hokkaido University, Sapporo 060, Japan

(Received November 9, 1985)

Abstract

We study twenty shallow earthquakes ($m_b \sim 6$) occurring at the junction of the Kurile and the Japan trenches for the period from 1964 to 1983 in order to understand the behavior of the oceanic and continental plate beneath the trench-arc system. Improved focal mechanisms and source depths of these events are simultaneously determined by the least square waveform inversion technique. The results show that the thrust faulting type is predominant throughout the region studied. These thrust events can be considered to be the interplate underthrust earthquakes between the downgoing slab and the overriding plate according to the following characteristics: their mechanisms are the same as that of the 1968 Tokachi-Oki earthquake; their slip vectors coincide with the motion direction of the Pacific plate; the depths of these events increase systematically with the distance between the epicenter of event and the trench axis; and the spatial distribution of these events from the trench axis continues smoothly to the upper envelope of the intermediate seismic zone in this region. The location of the thrust events represents the top of the downgoing slab.

A few events show the normal faulting type not only near the top of the downgoing slab but also within the slab. The former normal faulting events having the T axes nearly perpendicular to the trench axis can be explained by the bending of the oceanic plate. The latter events have the T axes approximately parallel to the trench axis and cannot be explained by the simple bending model of the oceanic plate. The events beneath the Hidaka Mountains in southern Hokkaido show the thrust faulting type different from the interplate earthquakes and they occurred within the overriding plate. Thus these events are not related to underthrusting of the Pacific plate, but may represent the relative motion of the Eurasian and North American plates at the triple junction proposed in this region. Above features indicate that, despite the bend of the trench axis at the junction of the Kurile and the Japan trenches, the underthrusting of the Pacific plate seems uniform, while the state of stress within the downgoing and the overriding plates are rather complex.

* Present address: Wakkanai Local Meteorological Observatory, Wakkanai 097, Japan.

1. Introduction

The spatial distribution and the focal mechanisms of earthquakes beneath a trench-island arc system are the most direct indications of the kinematic process now operating there. The location and dip of the major zone of thrust fault contact between the converging plates is indicated by the location of shallow earthquakes and by the plunges of the slip vectors derived from focal mechanisms (e.g. Isacks and Barazangi, 1977). The accurate determination of source depths and focal mechanisms, however, is difficult in the region between the trench and the island arc. Systematic errors in focal parameters cannot be excluded in this region because seismic stations are usually limited to the land area and complex lateral heterogeneity exists in the crust and upper mantle. The use of reflected phases (e.g. *pP* and *pwP*) gives more accurate source depths, if these phases can be clearly identified. Yoshii (1979 a) considered arrivals identified as *pP* in the International Seismological Center (ISC) Bulletin to be *pwP* and redetermined source depths of sub-oceanic earthquakes in the northeastern Japan. He found that scatter in locations was reduced and a two-planed seismic zone could be resolved. However, it is often difficult to distinguish between *pP* and *pwP* using short-period records alone (Forsyth, 1982 ; Hong and Fujita, 1981). Forsyth (1982) concluded from study of the techniques employed in determining depths of sub-oceanic earthquakes that one of the most powerful techniques for source depth determination was the modelling of long-period waveforms.

Focal mechanisms are usually determined by using body wave first motions. The first motions, however, have an intrinsic difficulty in that the very first motion of an earthquake may have nothing to do with the rest of the earthquake. The focal mechanism for the main rupture can be obtained from analysis of long-period waveforms. Recently, Langston (1976) and Wallace et al. (1981) presented a technique for the body wave inversion to determine the focal mechanism for the main rupture. Accurate focal mechanism determination is also necessary for the source depth determination by the waveform modelling technique. In this study, we try to determine simultaneously improved focal mechanisms and source depths by means of long-period body wave modelling in order to understand the behavior of the oceanic and continental plate beneath the trench-arc system.

We study twenty shallow earthquakes occurring at the junction of the Kurile and the Japan trenches (the ranges of latitude between 40°N and 43°N and of longitude between 142°E and 145°E) for the period from 1964 to 1983. The

Table 1 List of earthquakes studied.

Event No.	Date	Time h m	Lat. °N	Long. °E	Depth km	m_b
1	Jan. 10, 1964	04 50	41.85	142.78	57	6.1
2	June 13, 1965	07 06	41.72	143.60	37	5.7
3	Nov. 12, 1966	12 49	41.68	144.26	16	5.9
4	Jan. 06, 1967	00 04	41.80	143.39	41	5.6
5	Jan. 24, 1967	03 05	41.53	142.08	64	5.7
6	May 22, 1968	10 51	41.47	142.88	47	5.8
7	June 17, 1968	11 52	41.06	143.10	26	5.8
8	Sept. 21, 1968	13 06	42.08	142.65	57	5.9
9	Nov. 13, 1968	18 41	40.17	142.65	40	5.6
10	Jan. 20, 1970	17 33	42.48	143.04	25	6.3
11	May 27, 1970	22 35	40.24	143.08	29	5.6
12	Dec. 06, 1970	20 20	41.79	143.50	39	5.8
13	Aug. 02, 1971	07 24	41.37	143.44	45	6.5
14	Mar. 19, 1972	15 57	40.84	141.98	72	5.9
15	Jan. 24, 1974	19 12	42.03	143.89	27	5.8
16	Oct. 10, 1974	06 48	41.05	143.09	33	5.7
17	Sept. 19, 1975	17 54	41.86	142.76	52	5.6
18	Oct. 30, 1975	01 41	42.05	142.66	62	5.9
19	Feb. 20, 1979	06 32	40.22	143.55	46	5.9
20	Apr. 30, 1983	14 03	41.50	143.84	9	6.4

Earthquake data are from the ISC Bulletins.

epicenters of twenty events are shown in Fig. 1 and their focal parameters are listed in Table 1. These events have a body wave magnitude (m_b) of 5.6 to 6.4. The study area contains focal regions of two great earthquakes, the 1952 and 1968 Tokachi-Oki earthquakes (see the inset of Fig. 1).

2. Inversion procedure

We applied the least square waveform inversion technique proposed by Langston (1976) and Wallace et al. (1981) to determine the focal mechanism and the source depth of shallow earthquakes. The inversion technique makes use of an error function e defined as,

$$e=1-\phi(P_1, P_2, P_3, \ldots), \tag{1}$$

where $\phi(P_1, P_2, P_3, \ldots)$ is a cross correlation coefficient between the observed and synthetic seismograms and P_1, P_2, P_3, ... indicate the source parameters.

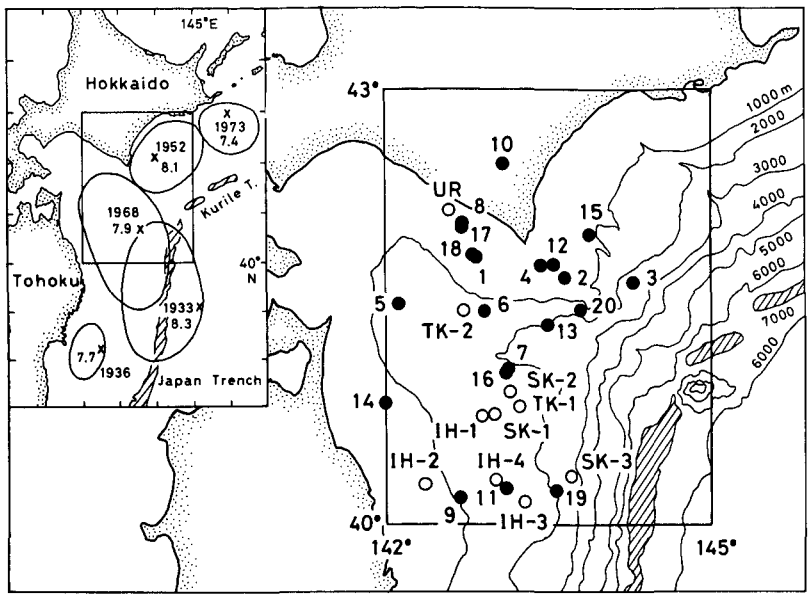

Fig. 1 Epicentral distribution of the earthquakes considered in this study. The epicenters determined by ISC are used. Solid circles are twenty events studied by the present authors. Open circles are the events studied by the previous authors; TK-1 and-2 by Kanamori (1971), IH-1～-4 by Izutani and Hirasawa (1978), SK-1～-3 by Seno and Kroeger (1983), and UR by Takeo et al. (1982). The numbers refer to the earthquakes listed in Tables 1 and 4. The map inset shows the focal regions of large earthquakes near the junction of the Kurile and the Japan trenches.

$\phi(P_1, P_2, P_3, \ldots)$ is defined as

$$\phi(P_1, P_2, P_3, \ldots)=\frac{\max\limits_{-\infty<\tau<\infty}\int_{-\infty}^{\infty} f(t)\, g(t+\tau\,;\, P_1, P_2, P_3, \ldots)dt}{\left[\int_{-\infty}^{\infty} f^2(t)dt \cdot \int_{-\infty}^{\infty} g^2(t\,;\, P_1, P_2, P_3, \ldots)dt\right]^{1/2}} \qquad (2)$$

where $f(t)$ is observed time series, $g(t\,;\, P_1, P_2, P_3, \ldots)$ is synthetic seismogram for the source parameters P_1, P_2, P_3, ..., and τ is a lag time. This technique involves an iteration method which minimize the root mean squares (RMS) of the error functions, that is,

$$RMS=\left(\sum_{j=1}^{N} e_j^2/N\right)^{1/2} \qquad (3)$$

where N is the number of the error functions. On each step, a parameter change is found according to Langston (1976) and Wallace et al. (1981). By the

very nature of the problem, noise introduces peculiar nonlinearities near the minimums in the model space. To counteract these effects the weighted parameter change as described by Langston (1976) is introduced to further convergence. The powerfulness of this waveform inversion technique was demonstrated by Wallace et al. (1981) and Miyamura (1985).

The synthetic seismogram $g(t)$ is determined using the relation

$$g(t)=G_{sk}\cdot s(t)*R_{sk}(t)*Q_k(t)*R_{rk}(t)*I(t), \quad (4)$$
$$k=P,\ SV,\ SH \text{ and } *=\text{convolution operator.}$$

Here G_s accounts for the effect of geometrical spreading within the mantle upon the amplitude of the body wave. $s(t)$ is the time history of the far-field body wave motion. $R_s(t)$ is the time history of the teleseismic mantle body wave due to an impulsive source within the layered medium used for the crust and upper mantle. In this study, we assume a point shear dislocation model. $R_s(t)$ is a function of the crustal model, the phase velocity of the teleseismic body wave, and the source parameters, that is, focal depth, strike of the fault plane, dip angle, and rake angle. The formulas of Bouchon (1976) are used to generate teleseismic body waves. $Q(t)$ accounts for the effect of anelastic attenuation in the mantle. We use the formula given by Aki and Richards (1980) in which $Q(t)$ is incorporated an average value of $T/\bar{Q}$, where T is the travel time and $\bar{Q}$ is the average quality factor along the particular path of the body wave. We take $T/\bar{Q}=1$ and $T/\bar{Q}=4$ for P and S waves, respectively, as a reasonable approximation for teleseismic body waves in the epicentral distance range of $\Delta=30°$ to $80°$. $R_r(t)$ is the response at the surface of the receiver crust for an incident impulsive teleseismic body wave. The response is calculated by using the propagator matrix given by Aki and Richards (1980). $I(t)$ is the impulse response of the seismograph system used. Hagiwara's (1958) formula for the response of an electromagnetic seismograph is used together with the appropriate constants.

The synthetic waveform changes with not only the source parameters but also the crust-upper mantle structure around the source region, through the factor $R_s(t)$ in (4). Especially the thickness of the sedimentary and water layers plays an important role in the synthetic waveform (Seno and Kroeger, 1983). Fortunately, several studies have been done on the sub-surface structure in the study area. Figure 2 shows the results obtained by Ludwig et al. (1966), Den et al. (1971), Asano et al. (1979, 1981), and Fujii and Moriya (1983). These results show a laterally varied crustal structure and a variation of the thickness of the sedimentary and water layers. Therefore, we assumed the different sub-

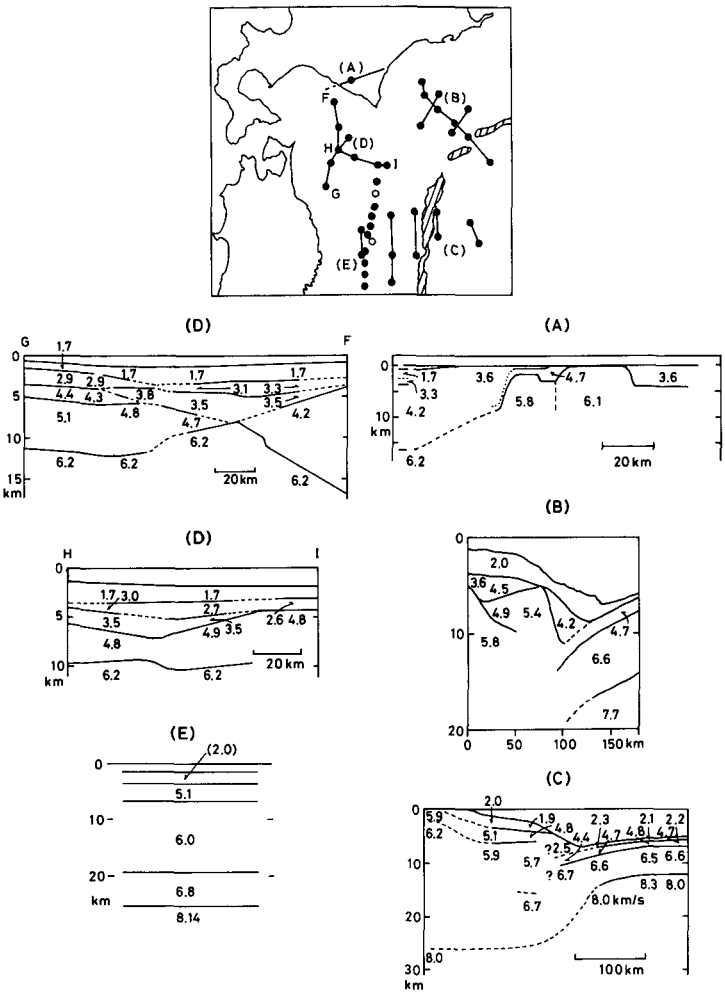

Fig. 2 Crustal structures revealed by seismic refraction studies. The profiles are shown in the inset. The original publications of the profiles are: (A)=Fujii and Moriya (1983); (B)=Den et al. (1971); (C)=Ludwig et al. (1966); (D)=Asano et al. (1979); and (E)=Asano et al. (1981). Numbers are *P* wave velocities in kilometers/second.

surface structure for each event according to the location of the event, referring to Fig. 2. The assumed crustal structures are summalized in Table 2. In this procedure we also referred to the gravity anomaly map given by Segawa (1970) and to the three dimensional velocity structure beneath the Hidaka Mountains by Takanami (1982) and Miyamachi and Moriya (1984).

Table 2 Crustal structures assumed for each event.

	V_p	V_s	ρ	H		V_p	V_s	ρ	H
No.1	1.50	0.0	1.03	0.2	No. 2	1.50	0.0	1.03	0.2
	2.00	1.15	2.00	3.0		2.00	1.15	2.00	1.0
	4.20	2.42	2.30	7.0		5.00	2.89	2.40	3.0
	6.00	3.47	2.60	11.0		5.80	3.35	2.50	10.0
	6.60	3.81	2.90	6.0		6.60	3.81	2.90	13.0
	8.10	4.68	3.30	∞		8.10	4.68	3.30	∞
No.3	1.50	0.0	1.03	2.4	No. 4	1.50	0.0	1.03	0.1
	2.00	1.15	2.00	1.0		2.00	1.15	2.00	1.0
	4.10	2.37	2.30	7.0		5.00	2.89	2.40	3.0
	5.80	3.35	2.50	10.0		5.80	3.35	2.50	10.0
	6.60	3.81	2.90	6.0		6.60	3.81	2.90	13.0
	8.10	4.68	3.30	∞		8.10	4.68	3.30	∞
No.5	1.50	0.0	1.03	1.2	No. 6	1.50	0.0	1.03	1.3
	2.00	1.15	2.00	3.0		2.00	1.15	2.00	3.0
	3.50	2.02	2.30	4.0		4.50	2.59	2.40	5.5
	6.20	3.58	2.60	8.0		6.20	3.58	2.60	7.0
	6.60	3.81	2.90	10.0		6.60	3.81	2.90	10.0
	8.10	4.68	3.30	∞		8.10	4.68	3.30	∞
No.7	1.50	0.0	1.03	1.9	No. 8	1.50	0.0	1.03	0.1
	2.00	1.15	2.00	2.0		2.00	1.15	2.00	3.0
	4.90	2.83	2.40	5.0		4.20	2.42	2.30	7.0
	6.20	3.58	2.60	11.0		6.00	3.47	2.60	11.0
	6.60	3.81	2.90	6.0		6.60	3.81	2.90	6.0
	8.10	4.68	3.30	∞		8.10	4.68	3.30	∞
No.9	1.50	0.0	1.03	1.1	No.10	6.10	3.63	2.80	15.0
	2.00	1.15	2.00	2.0		6.50	3.87	2.90	15.0
	5.10	2.94	2.40	4.0		7.70	4.58	3.20	20.0
	6.00	3.46	2.50	13.0		8.10	4.68	3.30	∞
	6.80	3.93	2.90	6.0					
	8.14	4.68	3.30	∞					

V_p=P wave velocity (km/s); V_s=S wave velocity (km/s);

WWSSN long-period P and SH waves were chosen for the waveform inversion. Stations used are between 30° and about 85° in order to avoid upper mantle structure effects. Approximate station locations relative to the epicentral region of twenty events are shown in the Appendix (Fig. A1). The actual procedure of the waveform inversion is as follows. First we made the starting model. The focal mechanism obtained by the previous study was

Table 2 Continued.

	V_p	V_s	ρ	H		V_p	V_s	ρ	H
No.11	1.50	0.0	1.03	1.3	No.12	1.50	0.0	1.03	0.1
	2.00	1.15	2.00	2.0		2.00	1.15	2.00	1.0
	5.10	2.94	2.40	3.0		5.00	2.89	2.40	3.0
	6.00	3.46	2.50	13.0		5.80	3.35	2.50	10.0
	6.80	3.93	2.90	6.0		6.60	3.81	2.90	13.0
	8.14	4.68	3.30	∞		8.10	4.68	3.30	∞
No.13	1.50	0.0	1.03	2.0	No.14	1.50	0.0	1.03	0.5
	2.00	1.15	2.00	2.0		3.00	1.73	2.20	4.5
	5.00	2.89	2.40	6.0		5.10	2.94	2.40	6.0
	5.90	3.41	2.50	10.0		6.20	3.58	2.60	6.0
	6.60	3.81	2.90	6.0		6.60	3.81	2.90	10.0
	8.10	4.68	3.30	∞		8.10	4.68	3.30	∞
No.15	1.50	0.0	1.03	0.8	No.16	1.50	0.0	1.03	1.9
	2.00	1.15	2.00	2.0		2.00	1.15	2.00	2.0
	5.00	2.89	2.40	3.0		4.90	2.83	2.40	5.0
	5.80	3.35	2.50	10.0		6.20	3.58	2.60	11.0
	6.60	3.81	2.90	13.0		6.60	3.81	2.90	6.0
	8.10	4.68	3.30	∞		8.10	4.68	3.30	∞
No.17	1.50	0.0	1.03	0.2	No.18	1.50	0.0	1.03	0.3
	2.00	1.15	2.00	3.0		2.00	1.15	2.00	3.0
	4.20	2.42	2.30	7.0		4.20	2.42	2.30	7.0
	6.00	3.47	2.60	11.0		6.00	3.47	2.60	11.0
	6.60	3.81	2.90	6.0		6.60	3.81	2.90	6.0
	8.10	4.68	3.30	∞		8.10	4.68	3.30	∞
No.19	1.50	0.0	1.03	2.0	No.20	1.50	0.0	1.03	1.7
	2.00	1.15	2.00	2.0		2.00	1.15	2.00	2.0
	5.10	2.94	2.40	2.0		5.00	2.89	2.40	6.0
	6.00	3.46	2.50	13.0		5.90	3.41	2.50	10.0
	6.80	3.93	2.90	6.0		6.60	3.81	2.90	6.0
	8.14	4.68	3.30	∞		8.10	4.68	3.30	∞

ρ = density (g/cm^3); H = thickness (km).

taken as the starting model. If there was no solution, we determine the mechanism on the basis of the P wave polarities and the S wave polarization angles obtained from the WWSSN long-period seismograms. Then the time history of the far-field body wave motion $s(t)$ was determined. In this study, $s(t)$ is taken to be an isosceles triangle with a base of T_s seconds. T_s was determined so that the first swing of the synthetic seismogram computed for the

starting model fitted the observed one. $s(t)$ is assumed to be independent of azimuth, which seems to be a good first approximation for earthquakes of this type of $m_b \sim 6$. Once the starting model and $s(t)$ were adopted, the waveform inversion was carried out for various source depths. Generally the first 50 sec of each record was used in the waveform inversion. The source parameters which gave the minimum *RMS* of the error functions was taken as the final medel. The seismic moment was finally calculated by comparing the amplitude of the synthetics and the observations.

3. Inversion results

The results of the waveform inversion are listed in Table 3. The comparison between the observed and synthetic seismograms are shown in the Appendix

Table 3 Results of the waveform inversion.

Event No.	Mechanism			Depth S.D.		Moment dyne-cm	T_s sec	Starting model
	Strike	Dip	Rake	km	km			
1	173°	17°	50°	44	2.6	1.7×10^{25}	5.0	Y
2	243°	30°	119°	26	3.7	0.44	3.0	Y
3	245°	14°	126°	18	1.9	0.48	5.0	Y
4	248°	19°	114°	34	1.1	0.43	4.0	N
5	206°	27°	97°	58	5.1	0.37	4.0	Y
6	264°	43°	−173°	46	3.5	0.47	4.0	Y
7	251°	21°	135°	24	4.8	2.6	6.0	Y
8	223°	16°	103°	52	3.6	9.5	6.0	Y
9	197°	28°	68°	32	3.7	1.4	5.0	Y
10	258°	29°	22°	34	2.6	7.7	6.0	Y
11	225°	24°	103°	22	1.9	0.73	5.0	N
12	261°	27°	135°	28	2.8	3.1	5.0	Y
13	108°	41°	− 81°	56	4.4	53.0	6.0	Y
14	337°	67°	− 5°	58	6.6	1.5	3.0	Y
15	231°	18°	116°	28	3.8	1.5	6.0	N
16	231°	34°	125°	32	5.2	2.0	4.0	N
17	177°	19°	67°	38	4.1	1.3	5.0	N
18	184°	15°	68°	50	3.0	1.8	5.0	N
19	67°	15°	− 49°	14	2.3	2.9	6.0	N
20	208°	34°	− 77°	18	2.0	1.9	5.0	N

S.D. denotes standard deviation of depth determination.
T_s is a base of isoceles triangle assumed for the far-field body wave time history.
Y=Yoshii's (1979 b) catalog; N=New solution.

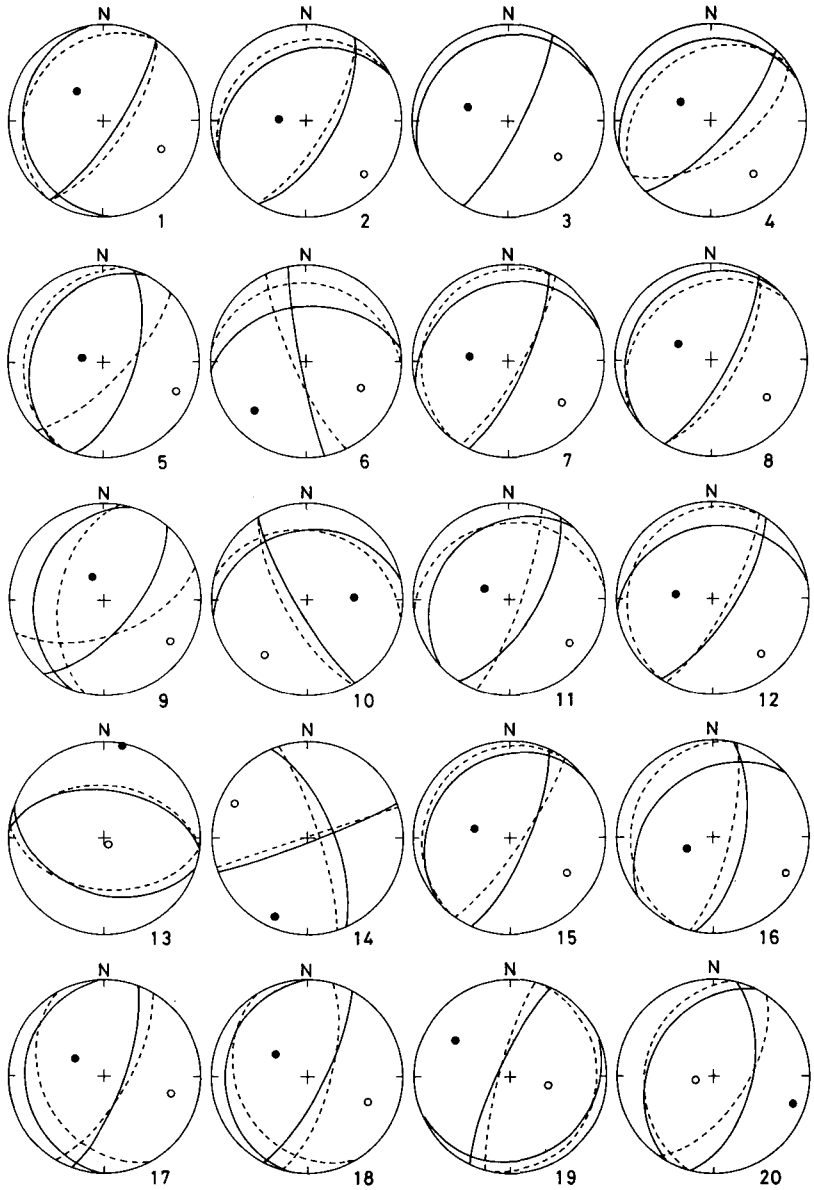

Fig. 3 Focal mechanism diagrams of twenty events studied. The mechanisms are equal-area projections of the lower focal hemisphere. Nodal lines are indicated by the solid lines and the dashed lines for the inversion solution and the starting model, respectively. In the diagram, an open circle represents the axis of compression and a solid circle, the axis of tension. Event numbers refer to Table 1.

(Fig. A2). The obtained focal mechanisms are shown in Fig. 3 using the equal area projection of the lower hemisphere. The dashed lines and the solid lines indicate the starting model and the inversion solution, respectively. In general, the discrepancy between both solutions is large for earthquakes with the starting model which was determined by using short-period data (Seno and Kroeger, 1983). Fifteen of twenty events are shown to be of the thrust faulting type.

Figure 4 illustrates the variation of *RMS* of the error functions with trial depth for two of the events studied. This figure shows that the depths are determined with the error of a few kilometers. The comparison of the depths determined in this study and those of the ISC routine determination is shown in Fig. 5 in a cross-section perpendicular to the local strike of the trench axis. The depths determined in this study are mostly shallower than those reported in ISC. This may be due to the effects of the low velocity sedimentary and water layers, which are really taken into account in our waveform modelling. As

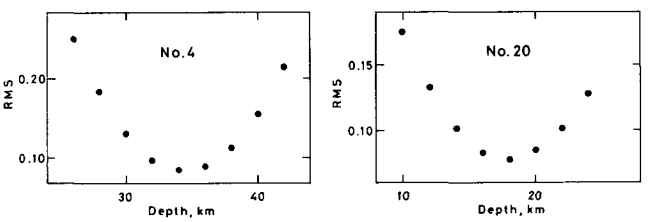

Fig. 4 Variation of *RMS* of the error functions with trial depth for events 4 and 20. Mechanisms used are the inversion solutions.

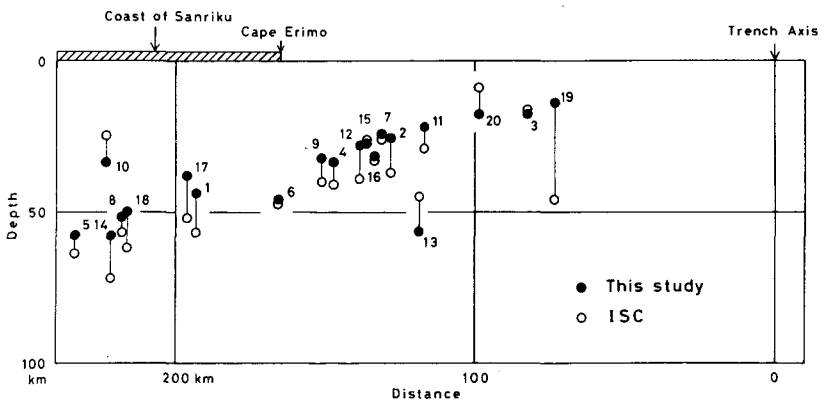

Fig. 5 Comparison of the foci obtained in this study (solid circles) and those by ISC (open circles) in the cross section perpendicular to the trench axis. Event numbers refer to Table 1.

shown in Fig. 8, scatter in locations determined by ISC for thrust events is considerably reduced by using the waveform inversion technique.

4. Discussion and conclusions

We discuss the tectonic implications of the results obtained in this study. The results show that the thrust faulting type is predominant throughout the study area. The focal mechanisms of the thrust events are shown in Fig. 6. Event 10, which is the thrust faulting type (see Fig. 3), is excluded from the figure because the mechanism is different from those in Fig. 6. In the figure, the results of thrust events studied by Izutani and Hirasawa (1978) and Seno and Kroeger (1983) are also shown. The focal mechanisms and source depths of

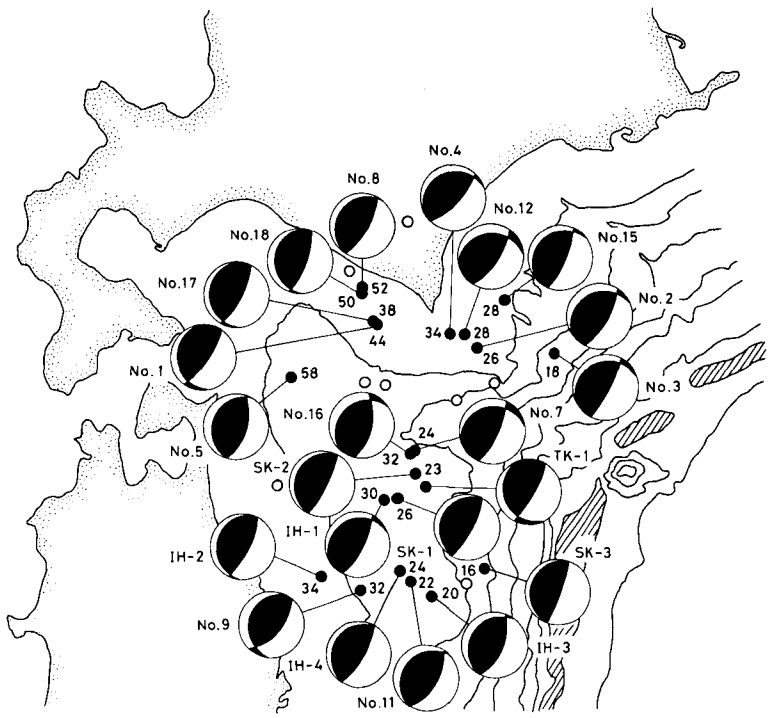

Fig. 6 Focal mechanisms of the interplate underthrust earthquakes. The shaded areas indicate the compressional quadrants. Event numbers refer to Tables 1 and 4. TK-1 is the main shock of the 1968 Tokachi-Oki earthquake (Kanamori, 1971). The number attached to each epicenter is the source depth in kilometers. Open circles are epicenters of events whose mechanisms are different from those presented in this figure.

Table 4 Earthquake data studied by the previous authors

Event	Date	Time h m	Lat. °N	Long. °E	Depth km	m_b	Mechanism		
							Strike	Dip	Rake
SK-1	Mar. 16.1965	16 46	40.75	142.96	26	5.8	208°	14°	90°
SK-2	May. 24.1968	14 06	40.91	143.11	23	5.7	208°	10°	90°
SK-3	June 22.1968	01 12	40.31	143.68	16	5.6	201°	6°	90°
IH-1	Mar. 29.1965	10 47	40.73	142.85	30	6.1	247°	18°	128°
IH-2	May 22.1968	19 29	40.27	142.34	34	5.3	215°	24°	103°
IH-3	Nov. 11.1968	14 41	40.12	143.25	20	5.5	219°	14°	97°
IH-4	May 27.1970	19 05	40.29	142.98	24	5.7	194°	16°	77°
TK-1	May 16.1968	00 48	40.86	143.38	9*	6.1	156°	20°	37°
TK-2	May 16.1968	10 39	41.52	142.82	24**	6.4	201°	11°	−125°
UR	Mar. 21.1982	02 32	42.23	142.46	26*	6.3	150°	50°	110°

SK=Seno Kroeger (1983); IH=Izutani and Hirasawa (1978); TK=Kanamori (1971); UR=Takeo et al. (1982). Epicenters are from the ISC Bulletins. *=after ISC. **=after preliminary our study.

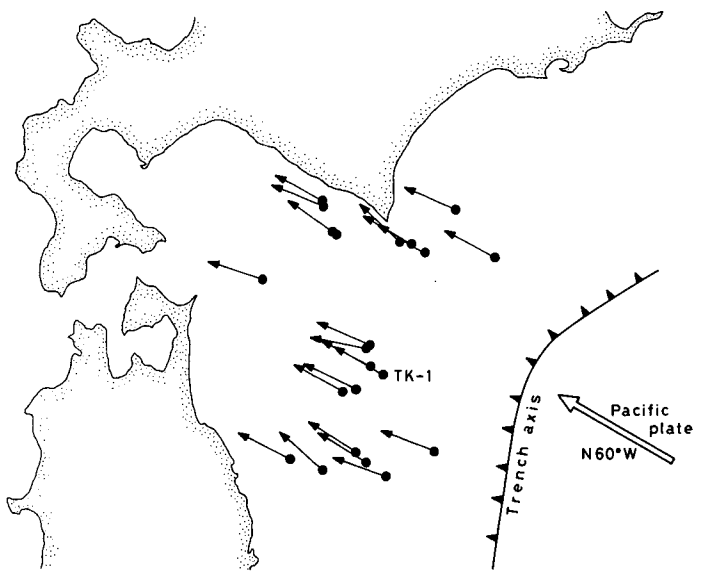

Fig. 7 Slip vectors of the interplate events shown in Fig. 6. The motion direction of the Pacific plate is represented by a large arrow.

these events were obtained based on the waveform modelling as used in this study. TK-1 is the focal mechanism of the great Tokachi-Oki earthquake of 1968 studied by Kanamori (1971). Data of these events studied by the previous authors are listed in Table 4. As shown in Fig. 6, the thrust events have the

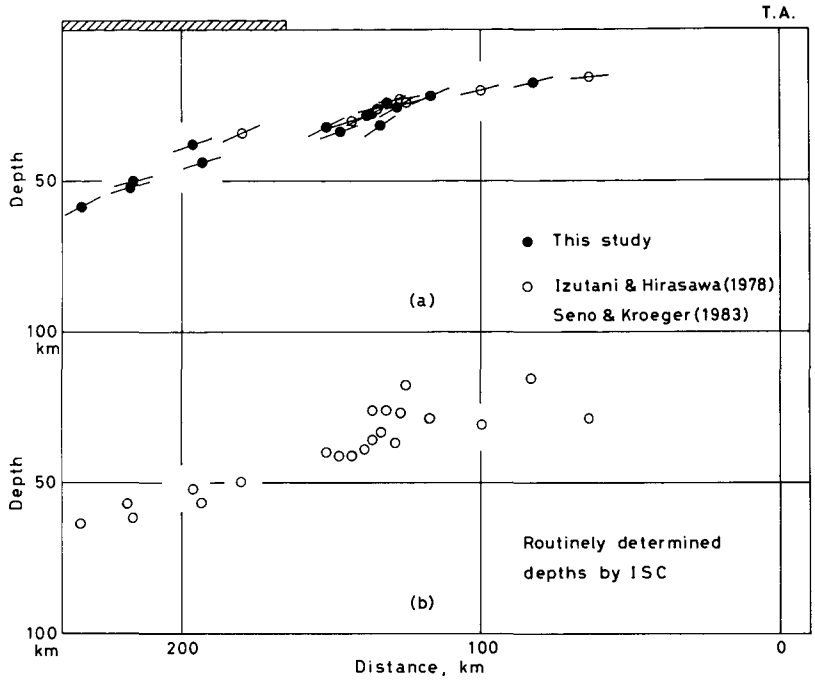

Fig. 8 Foci of the interplate events in the cross section perpendicular to the trench axis. (a) Foci obtained in this study and those by Izutani and Hirasawa (1978) and Seno and Kroeger (1983). A bar attached to each circle indicates the dip of the fault plane. (b) Routinely determined depths by ISC. T.A. indicates the trench axis.

focal mechanisms similar to that of TK-1. The Tokachi-Oki earthquake is known as the interplate underthrust event at the interface between the downgoing slab and the overriding plate (Kanamori, 1971). Therefore, we consider that these thrust events are also the interplate earthquakes. In fact, the slip vectors of the thrust events, which show the direction of the motion of the foot-wall side with respect to the hanging wall side, have almost the same direction (Fig. 7; average direction of N62°W) and coincide with the motion direction of the Pacific plate by Minster and Jordan (1978). Figure 7 also shows that, despite the bend of the trench axis at the junction of the Kurile and the Japan trenches, the displacement of the Pacific plate seems relatively uniform at least in this region.

Figure 6 shows that the depths of the thrust events increase systematically with the distance between the epicenter of event and the trench axis. This can be clearly seen in Figure 8(a) which shows the foci of the thrust events in the

cross-section perpendicular to the strike of the trench axis. Fig. 8(b) shows the similar cross-section whereas the foci determined by ISC are used. Scatter in locations in Fig. 8(b) is considerably reduced by using the waveform inversion technique (Fig. 8(a)). Also shown in Fig. 8(a) are the fault planes of the thrust events. We take the gently dipping nodal plane of the mechanism solution as the fault plane. The dips of the fault planes increase more or less with depths and the fault planes construct a smoothly curved surface slightly dipping toward the island arc. This curved surface may be considered to be the interface between the downgoing slab and the overriding plate and we suggest that the Tokachi-Oki earthquake just occurred along this surface.

Recent seismicity studies have indicated that double seismic zones of intermediate-depth earthquakes exist in the depth ranges of 70-180 km beneath northeastern Honshu and the middle of Hokkaido (Umino and Hasegawa, 1975; Takagi et al., 1977; Yoshii, 1979 a; Suzuki et al., 1983). It is interesting to investigate the relationship between the double seismic zone and the plate interface suggested. Figure 9 shows the spatial distribution of microearthquakes obtained by Suzuki et al. (1983; profile X-X′ in their Fig. 4) with the foci of the thrust events obtained in this study. In Fig. 9, we omit the sub-oceanic microearthquakes from their original figure because of less reliable hypocenter determinations. It can be seen that the spatial distribution of the thrust events continues smoothly to the upper plane of the double-planed intermediate seismic zone. This evidently indicates the geometry of the top of the downgoing slab. In the previous studies, the top of the downgoing slab was approximately

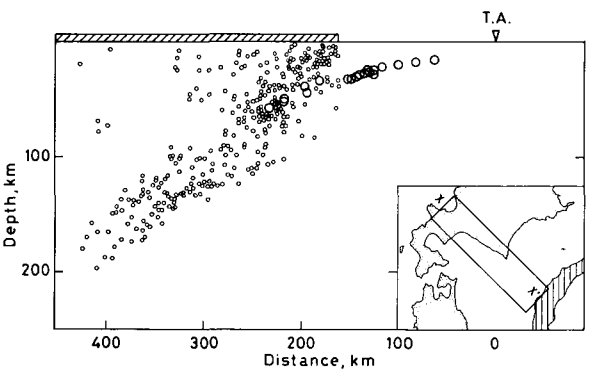

Fig. 9 Comparison of the foci of the interplate events (large circles) and those of microearthquakes (small circles) revised from Suzuki et al. (1983), in the cross section perpendicular to the trench axis. The microearthquakes occurring in the rectangular area in the map inset are shown, but offshore microearthquakes are omitted.

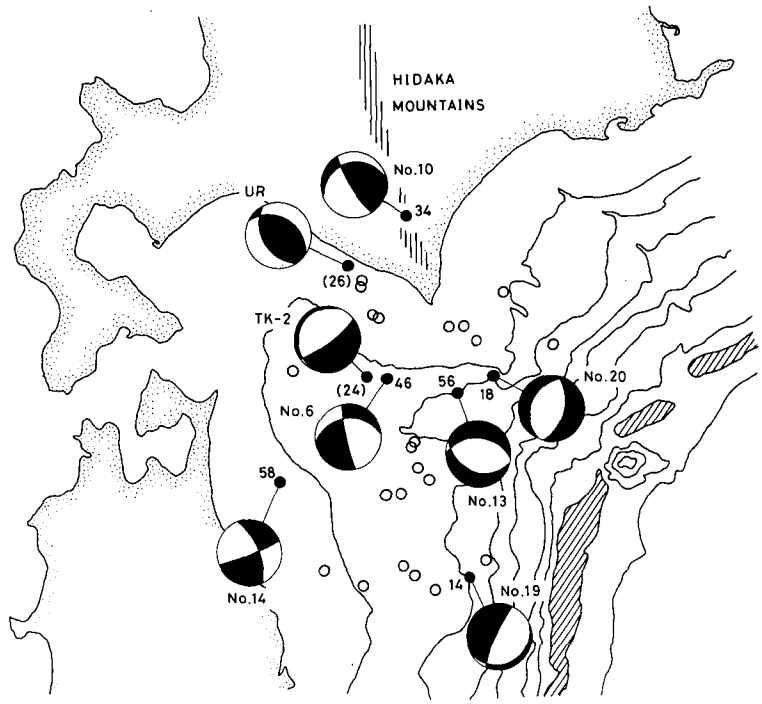

Fig. 10 (a) Focal mechanisms of events except the interplate events. The shaded areas indicate the compressional quadrants. Event numbers refer to Tables 1 and 4. TK-2 is the largest aftershock of the 1968 Tokachi-Oki earthquake (Kanamori, 1971) and UR is the 1982 Urakawa-Oki earthquake (Takeo et al., 1982). The number attached to each epicenter is the source depth in kilometers. (b) Foci of the events shown in (a) (open circles) in the cross section perpendicular to the trench axis. Also shown are the foci of the interplate events (solid circles).

estimated based upon the distribution of routinely determined hypocenters.

Figure 10(a) shows the focal mechanisms of the events which are not regarded as the interplate underthrust earthquakes. Mechanisms of the largest aftershock of the 1968 Tokachi-Oki earthquake (TK-2 ; Kanamori, 1971) and the Urakawa-Oki earthquake of 1982 (UR ; Takeo et al., 1982) are also included in the figure. Their foci are shown in the cross-section perpendicular to the trench axis in Fig. 10(b). Five of twenty events studied here show the normal faulting type. Mechanisms of these events are not similar to that of the normal faulting event TK-2 occurring near the suggested plate interface, which Kanamori (1971) has attributed to complex interactions among three plates (the northeastern Japan plate, the Hokkaido plate and the Pacific plate) at the junction of the Japan and the Kurile trenches. Events 19 and 20 have the T axes approximately perpendicular to the trench axis and occurred near the plate interface. Thus these two events can be explained by the bending of the oceanic plate, although the hypocenters are located beneath the landward wall of the trench (Stauder, 1968 ; Chapple and Forsyth, 1979). The bending of the oceanic plate near the trench predicts horizontal deviatoric compression within the interior of the plate, as deep as 40-50 km within the bending plate (e.g., Chapple and Forsyth, 1979). However, event 13 which is located to be about 40 km below the plate interface indicates the normal faulting type and its T axis is approximately parallel to the trench axis. Events 6 and 14 which occurred more or less within the oceanic plate have the T axes with approximately the same direction as that of event 13. These normal faulting events cannot be explained by the simple bending model of the oceanic plate. At the junction of the Kurile and the Japan trenches, the stress field within the oceanic plate is characterized by the horizontal T axes which are approximately parallel to the trench axis. The normal faulting events inside the downgoing slab have been found in the Chilean subduction zone (Malgrange and Madariaga, 1983) ; however, the T axes of the Chilean normal faulting events are perpendicular to the trench axis.

Events 10 and UR beneath the Hidaka Mountains in southern Hokkaido show the thrust faulting type. Their focal mechanisms are quite different from those of the interplate earthquakes shown in Fig. 6. Figure 10(b) shows that these events occurred at depths shallower than the plate interface. Then events 10 and UR are regarded as the intraplate earthquakes within the overriding plate. Yoshii (1979 a) summalized the focal mechanisms around northeastern Honshu and showed that the events occurring within the overriding plate had horizontal compressions perpendicular to the trench axis. The P axes of

events 10 and UR, however, are approximately parallel to the trench axis. Kasahara (1984) showed the contraction in the direction of ENE to WSW around the southern part of the Hidaka Mountains from the geodetic observations. His result is approximately consistent with the direction of the P axes of events 10 and UR. We consider events 10 and UR to be unrelated to underthrusting of the Pacific plate because of their shallow depths and because of the orientation of the focal mechanisms. Den and Hotta (1973) and Chapman and Solomon (1976) proposed the existence of a triple junction of the Eurasian, Pacific and North American (or Okhotsk) plates in the study area. Events 10 and UR may represent the relative motion of the Eurasian and North American plates (Chapman and Solomon, 1976).

Appendix: Comparison of the Observed and Synthetic P and SH waves

We present here approximate station locations relative to the epicentral region of twenty events studied (Fig. A1) and comparisons of the observed and synthetic P and SH waves for these events (Fig. A2).

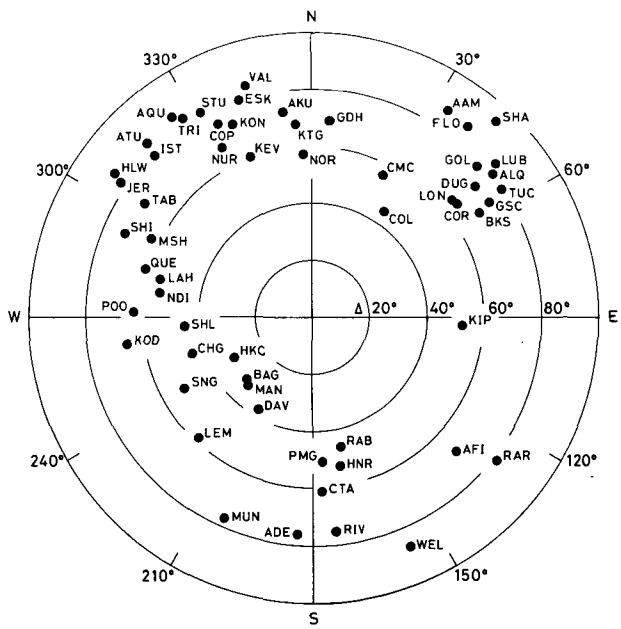

Fig. A1 Approximate station locations relative to the epicentral region of twenty events. Concentric circles show epicentral distances.

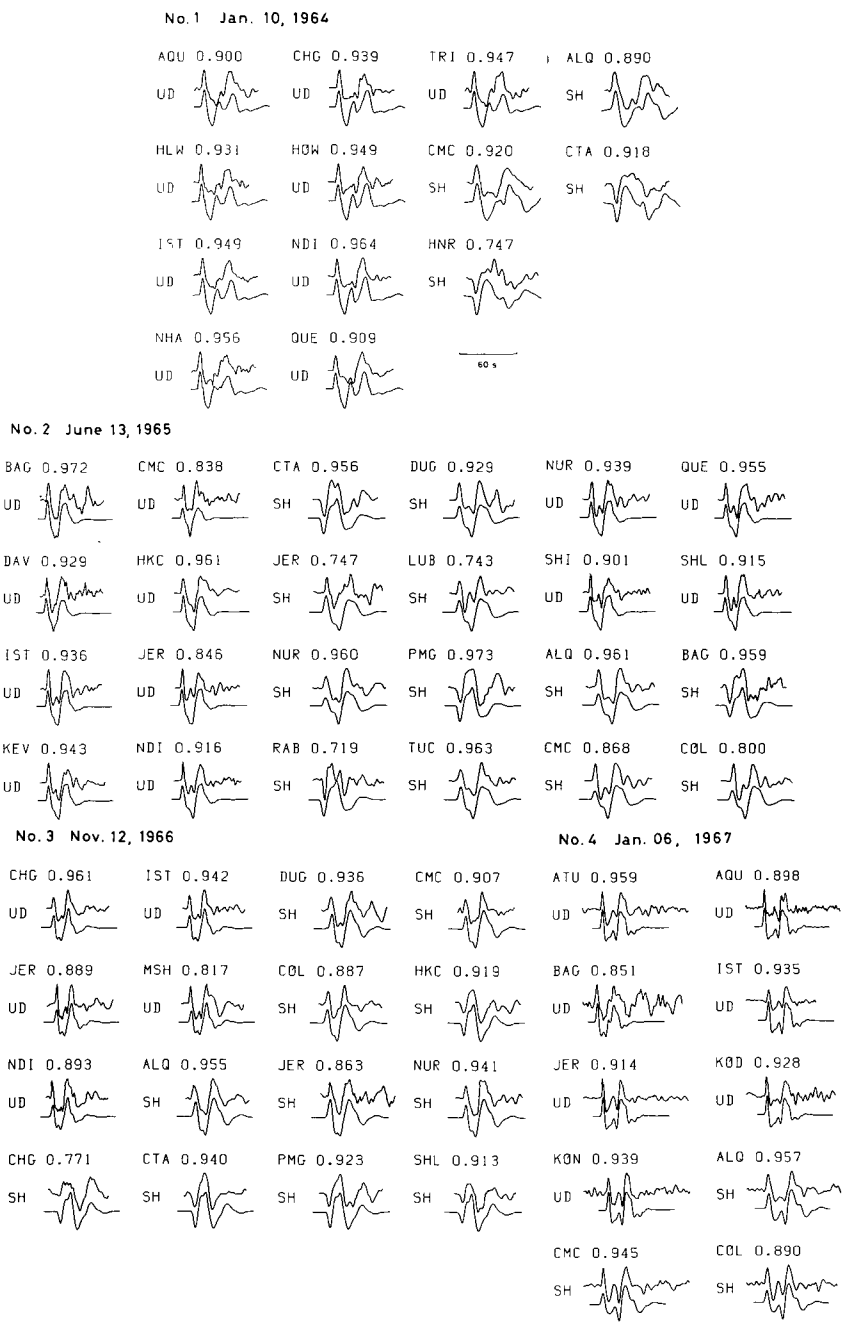
No. 1 Jan. 10, 1964
AQU 0.900
UD
CHG 0.939
UD
TRI 0.947
UD
ALQ 0.890
SH
HLW 0.931
UD
HOW 0.949
UD
CMC 0.920
SH
CTA 0.918
SH
IST 0.949
UD
NDI 0.964
UD
HNR 0.747
SH
NHA 0.956
UD
QUE 0.909
UD
60 s
No. 2 June 13, 1965
BAG 0.972
UD
CMC 0.838
UD
CTA 0.956
SH
DUG 0.929
SH
NUR 0.939
UD
QUE 0.955
UD
DAV 0.929
UD
HKC 0.961
UD
JER 0.747
SH
LUB 0.743
SH
SHI 0.901
UD
SHL 0.915
UD
IST 0.936
UD
JER 0.846
UD
NUR 0.960
SH
PMG 0.973
SH
ALQ 0.961
SH
BAG 0.959
SH
KEV 0.943
UD
NDI 0.916
UD
RAB 0.719
SH
TUC 0.963
SH
CMC 0.868
SH
COL 0.800
SH
No. 3 Nov. 12, 1966
CHG 0.961
UD
IST 0.942
UD
DUG 0.936
SH
CMC 0.907
SH
JER 0.889
UD
MSH 0.817
UD
COL 0.887
SH
HKC 0.919
SH
NDI 0.893
UD
ALQ 0.955
SH
JER 0.863
SH
NUR 0.941
SH
CHG 0.771
SH
CTA 0.940
SH
PMG 0.923
SH
SHL 0.913
SH
No. 4 Jan. 06, 1967
ATU 0.959
UD
AQU 0.898
UD
BAG 0.851
UD
IST 0.935
UD
JER 0.914
UD
KOD 0.928
UD
KON 0.939
UD
ALQ 0.957
SH
CMC 0.945
SH
COL 0.890
SH

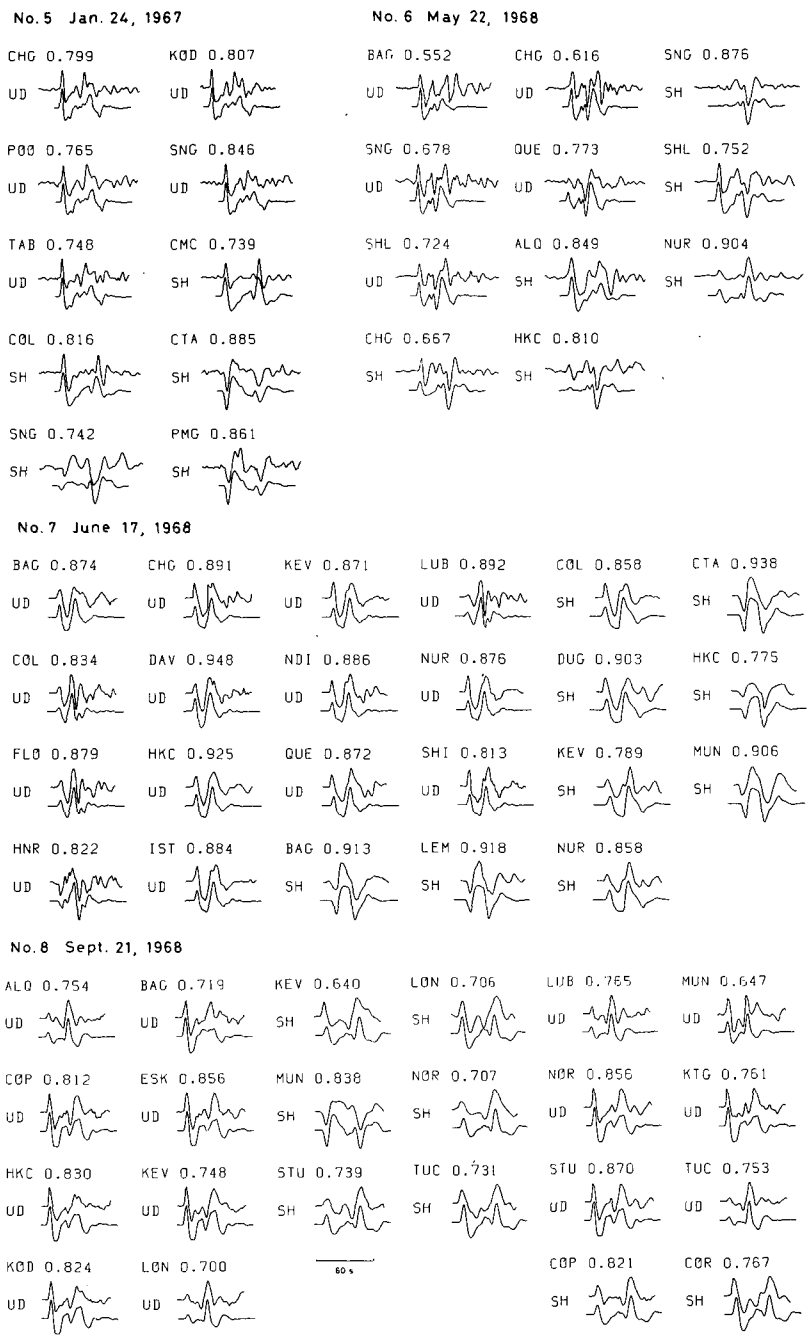
No. 5 Jan. 24, 1967
CHG 0.799
UD
KØD 0.807
UD
PØØ 0.765
UD
SNG 0.846
UD
TAB 0.748
UD
CMC 0.739
SH
CØL 0.816
SH
CTA 0.885
SH
SNG 0.742
SH
PMG 0.861
SH
No. 6 May 22, 1968
BAG 0.552
UD
CHG 0.616
UD
SNG 0.876
SH
SNG 0.678
UD
QUE 0.773
UD
SHL 0.752
SH
SHL 0.724
UD
ALQ 0.849
SH
NUR 0.904
SH
CHG 0.667
SH
HKC 0.810
SH
No. 7 June 17, 1968
BAG 0.874
UD
CHG 0.891
UD
KEV 0.871
UD
LUB 0.892
UD
CØL 0.858
SH
CTA 0.938
SH
CØL 0.834
UD
DAV 0.948
UD
NDI 0.886
UD
NUR 0.876
UD
DUG 0.903
SH
HKC 0.775
SH
FLØ 0.879
UD
HKC 0.925
UD
QUE 0.872
UD
SHI 0.813
UD
KEV 0.789
SH
MUN 0.906
SH
HNR 0.822
UD
IST 0.884
UD
BAG 0.913
SH
LEM 0.918
SH
NUR 0.858
SH
No. 8 Sept. 21, 1968
ALQ 0.754
UD
BAG 0.719
UD
KEV 0.640
SH
LØN 0.706
SH
LUB 0.765
UD
MUN 0.647
UD
CØP 0.812
UD
ESK 0.856
UD
MUN 0.838
SH
NØR 0.707
SH
NØR 0.856
UD
KTG 0.761
UD
HKC 0.830
UD
KEV 0.748
UD
STU 0.739
SH
TUC 0.731
SH
STU 0.870
UD
TUC 0.753
UD
KØD 0.824
UD
LØN 0.700
UD
60 s
CØP 0.821
SH
CØR 0.767
SH

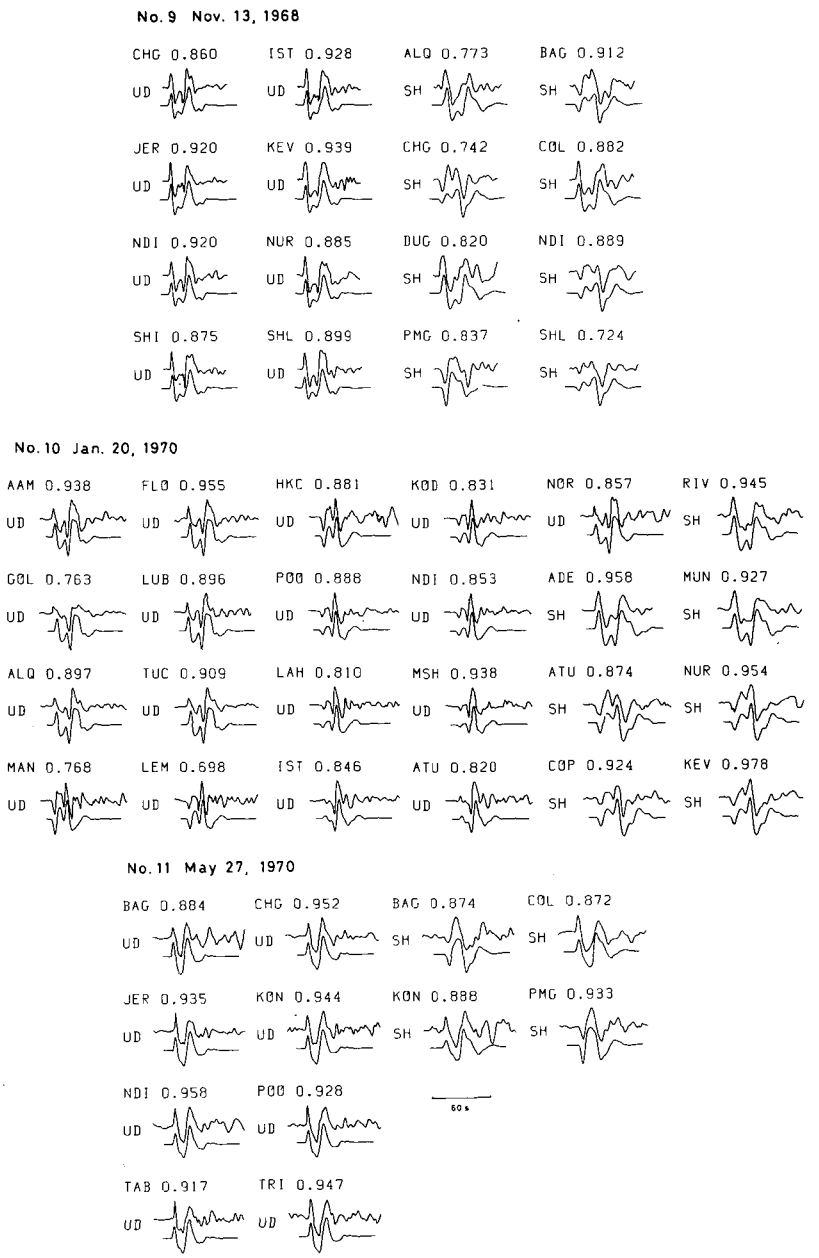
No. 9 Nov. 13, 1968
CHG 0.860
UD
IST 0.928
UD
ALQ 0.773
SH
BAG 0.912
SH
JER 0.920
UD
KEV 0.939
UD
CHG 0.742
SH
COL 0.882
SH
NDI 0.920
UD
NUR 0.885
UD
DUG 0.820
SH
NDI 0.889
SH
SHI 0.875
UD
SHL 0.899
UD
PMG 0.837
SH
SHL 0.724
SH
No. 10 Jan. 20, 1970
AAM 0.938
UD
FLØ 0.955
UD
HKC 0.881
UD
KØD 0.831
UD
NOR 0.857
UD
RIV 0.945
SH
GØL 0.763
UD
LUB 0.896
UD
PØØ 0.888
UD
NDI 0.853
UD
ADE 0.958
SH
MUN 0.927
SH
ALQ 0.897
UD
TUC 0.909
UD
LAH 0.810
UD
MSH 0.938
UD
ATU 0.874
SH
NUR 0.954
SH
MAN 0.768
UD
LEM 0.698
UD
IST 0.846
UD
ATU 0.820
UD
CØP 0.924
SH
KEV 0.978
SH
No. 11 May 27, 1970
BAG 0.884
UD
CHG 0.952
UD
BAG 0.874
SH
COL 0.872
SH
JER 0.935
UD
KØN 0.944
UD
KØN 0.888
SH
PMG 0.933
SH
NDI 0.958
UD
PØØ 0.928
UD
60 s
TAB 0.917
UD
TRI 0.947
UD

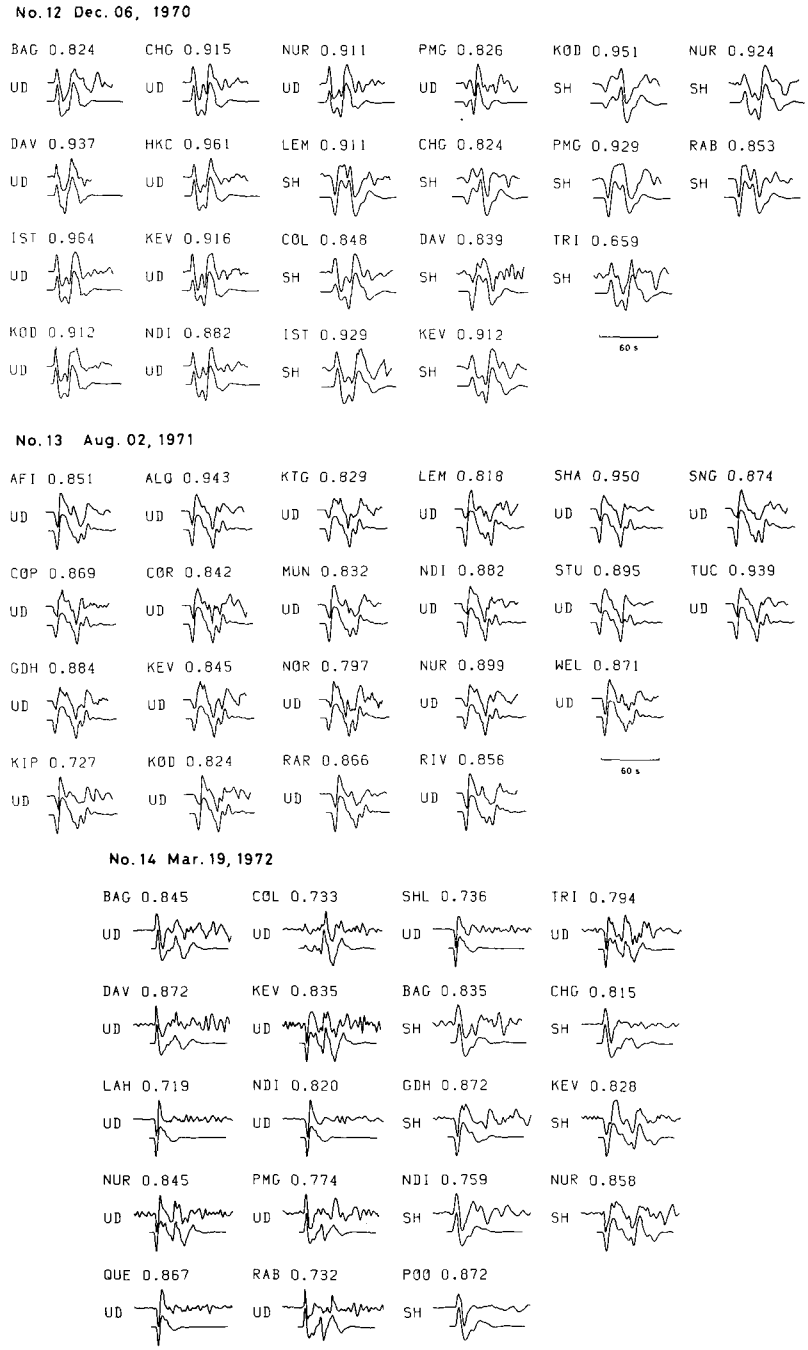
No. 12 Dec. 06, 1970
BAG 0.824
UD
CHG 0.915
UD
NUR 0.911
UD
PMG 0.826
UD
KØD 0.951
SH
NUR 0.924
SH
DAV 0.937
UD
HKC 0.961
UD
LEM 0.911
SH
CHG 0.824
SH
PMG 0.929
SH
RAB 0.853
SH
IST 0.964
UD
KEV 0.916
UD
COL 0.848
SH
DAV 0.839
SH
TRI 0.659
SH
KØD 0.912
UD
NDI 0.882
UD
IST 0.929
SH
KEV 0.912
SH
60 s
No. 13 Aug. 02, 1971
AFI 0.851
UD
ALQ 0.943
UD
KTG 0.829
UD
LEM 0.818
UD
SHA 0.950
UD
SNG 0.874
UD
COP 0.869
UD
COR 0.842
UD
MUN 0.832
UD
NDI 0.882
UD
STU 0.895
UD
TUC 0.939
UD
GDH 0.884
UD
KEV 0.845
UD
NOR 0.797
UD
NUR 0.899
UD
WEL 0.871
UD
KIP 0.727
UD
KØD 0.824
UD
RAR 0.866
UD
RIV 0.856
UD
60 s
No. 14 Mar. 19, 1972
BAG 0.845
UD
COL 0.733
UD
SHL 0.736
UD
TRI 0.794
UD
DAV 0.872
UD
KEV 0.835
UD
BAG 0.835
SH
CHG 0.815
SH
LAH 0.719
UD
NDI 0.820
UD
GDH 0.872
SH
KEV 0.828
SH
NUR 0.845
UD
PMG 0.774
UD
NDI 0.759
SH
NUR 0.858
SH
QUE 0.867
UD
RAB 0.732
UD
P00 0.872
SH

No. 15 Jan. 24, 1974

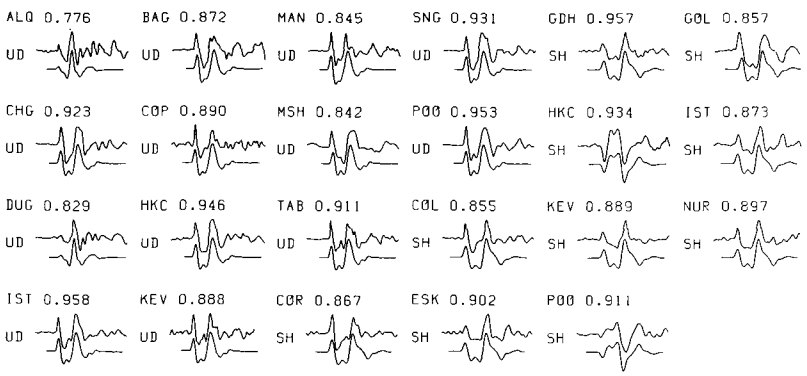

No. 16 Oct. 10, 1974

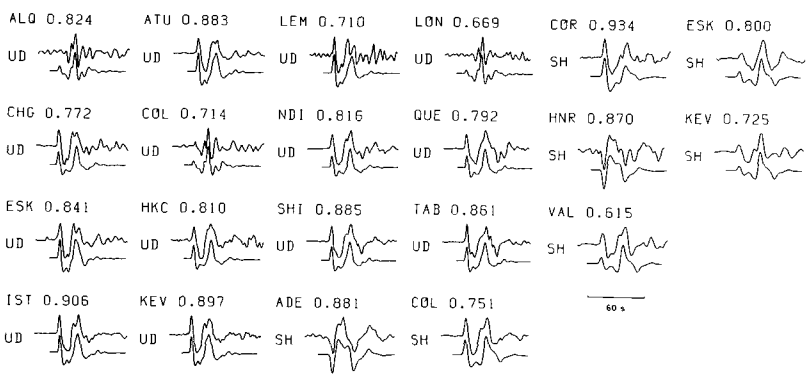

No. 17 Sept. 19, 1975

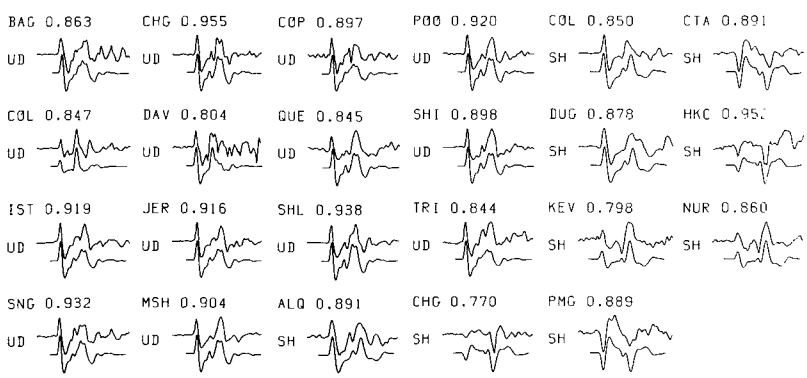

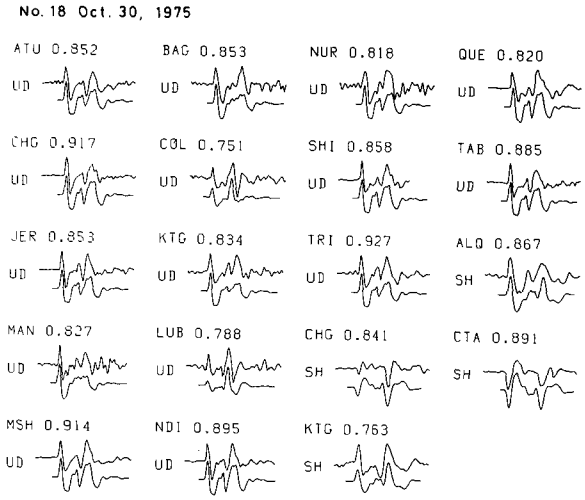
No. 18 Oct. 30, 1975
ATU 0.852
UD
BAG 0.853
UD
NUR 0.818
UD
QUE 0.820
UD
CHG 0.917
UD
COL 0.751
UD
SHI 0.858
UD
TAB 0.885
UD
JER 0.853
UD
KTG 0.834
UD
TRI 0.927
UD
ALQ 0.867
SH
MAN 0.827
UD
LUB 0.788
UD
CHG 0.841
SH
CTA 0.891
SH
MSH 0.914
UD
NDI 0.895
UD
KTG 0.763
SH

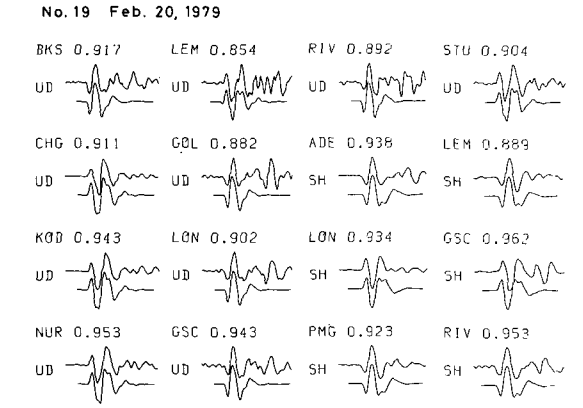
No. 19 Feb. 20, 1979
BKS 0.917
UD
LEM 0.854
UD
RIV 0.892
UD
STU 0.904
UD
CHG 0.911
UD
GOL 0.882
UD
ADE 0.938
SH
LEM 0.889
SH
KOD 0.943
UD
LON 0.902
UD
LON 0.934
SH
GSC 0.962
SH
NUR 0.953
UD
GSC 0.943
UD
PMG 0.923
SH
RIV 0.953
SH

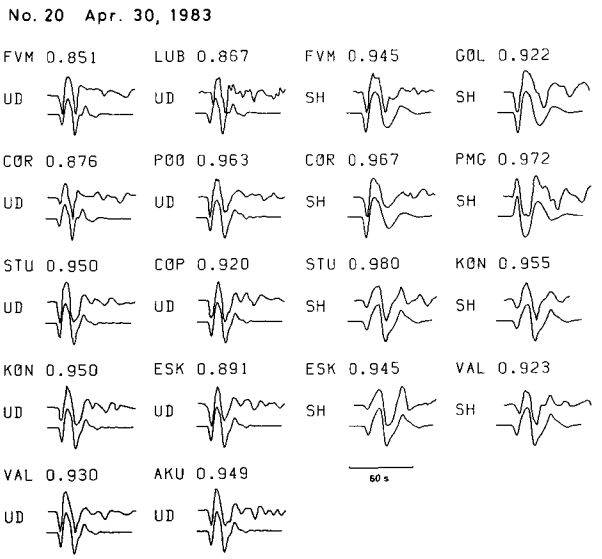

Fig. A2 Comparison of the observed (upper trace) and synthetic (lower trace) long-period *P* and *SH* waves. Numbers indicate the cross-correlation coefficients between the observed and synthetic seismograms.

Acknowledgements

The authors are much indebted to Prof. Hs. Okada and Dr. T. Moriya for stimulating discussions and helpful comments. We wish to thank Dr. T. Iwasaki for his valuable advices. We also thank Dr. K. Shimazaki of the Earthquake Research Institute, the University of Tokyo, for his assistance in collecting the WWSSN data.

The numerical computations were carried out by HITAC M280H at the Hokkaido University Computing Center.

References

Aki, K. and P.G. Richards, 1980. Quantitative seismology. vol. 1, pp 1-557, W.H. Freeman and Company.

Asano, S., N. Den, H. Hotta, T. Yoshii, Y. Ichinose, N. Sakajiri and T. Sasatani, 1979. Seismic refraction and reflection measurements around Hokkaido. Part 2. Crustal structure at the continental slope off Hidaka. J. Phys. Earth, **27**, 497-509.

Asano, S., T. Yamada, K. Suyehiro, T. Yoshii, Y. Misawa and S. Iizuka, 1981. Crustal structure in a profile off the Pacific coast of northeastern Japan by refraction method using

ocean bottom seismometers. J. Phys. Earth, **29**, 267-282.
Bouchon, M., 1976. Teleseismic body wave radiation from a seismic source in a layered medium. Geophys. J.R. astr. Soc., **47**, 515-530.
Chapman, M.E. and S.C. Solomon, 1976. North American-Eurasian plate boundary in Northeast Asia. J. Geophys. Res., **81**, 921-930.
Chapple, W.M. and D.W. Forsyth, 1979. Earthquakes and bending of plates at trenches. J. Geophys. Res., **84**., 6729-6749.
Den, N., H. Hotta, S. Asano, T. Yoshii, N. Sakajiri, Y. Ichinose, M. Motoyama, K. Kakiichi, A. F. Beresnev and A.A. Sagalevitch, 1971. Seismic refraction and reflection measurements around Hokkaido. Part 1. Crustal structure of the continental slope off Tokachi. J. Phys. Earth, **19**, 329-345.
Den, N. and H. Hotta, 1973. Seismic refraction and reflection evidence supporting plate tectonics in Hokkaido. Pap. Meteorol. Geophys., **24**, 31-54.
Forsyth, D.W., 1982. Determinations of focal depths of earthquakes associated with the bending of oceanic plates at trenches. Phys. Earth Planet. Int., **28**, 141-160.
Fujii, S. and T. Moriya, 1983. Velocity structure in the Hidaka district by the quarry blast. Geophys. Bull. Hokkaido Univ., **42**, 145-154 (in Japanese).
Hagiwara, T., 1958. A note on the theory of the electromagnetic seismograph. Bull. Earthq. Res. Inst., **44**, 139-164.
Hong, T.-L., and K. Fujita, 1981. Modelling of depth phases and source processes of some central Aleutian earthquakes. Earth Planet. Sci. Lett., **53**, 333-342.
Isacks, B. and M. Barazangi, 1977. Geometry of Benioff zones: lateral segmentation and downward bending of the subducted lithosphere. In: M. Talwani and W.C. Pitman III (Editors), Island Arcs, Deep Sea Trenches and Back-Arc Basins. Am. Geophys. Union, Washington, D.C., pp. 99-114.
Izutani, Y. and T. Hirasawa, 1978. Source characteristics of shallow earthquakes in the northern part of Sanriku-Oki region, Japan. J. Phys. Earth, **26**, 275-297.
Kanamori, H., 1971. Focal mechanism of the Tokachi-Oki earthquake of May 16, 1968: contortion of the lithosphere at a junction of two trenches. Tectonophysics, **12**, 1-13.
Kasahara, M., 1984. Horizontal strain accumulated in the Erimo region Hokkaido, from 1971 to 1980 obtained by geodetic and extensometric observations. J. Fac. Sci., Hokkaido Univ., Ser. VII (Geophys), **7**, 327-338.
Langston, C.A., 1976. A body wave inversion of the Koyna India, earthquake of December 10, 1967, and some implications for body wave focal mechanisms. J. Geophys. Res., **81**, 2517-2529.
Ludwig, W.J., J.I. Ewing, M. Ewing, S. Murauchi, N. Den, S. Asano, H. Hotta, M. Hayakawa, T. Asanuma, K. Ichikawa, and I. Noguchi. Sediments and structure of the Japan trench. J. Geophys. Res., **71**, 2121-2137.
Malgrange, M. and R. Madariaga, 1983. Complex distribution of large thrust and normal fault earthquakes in the Chilean subduction zone. Geophys. J.R. astr. Soc., **73**, 489-505.
Minster, J.B. and T.H. Jordan, 1978. Present-day plate motions. J. Geophys. Res., **83**, 5331-5354.
Miyamachi, H. and T. Moriya, 1984. Velocity structure beneath the Hidaka Mountains in Hokkaido, Japan. J. Phys. Earth, **32**, 13-42.
Miyamura, J., 1985. Determination of focal mechanisms and source depths using waveform analysis of long-period body waves: Shallow earthquakes at a junction between the Kurile and the Japan trenches. Master thesis, Hokkaido Univ., pp. 1-178 (in Japanese).
Segawa, J., 1970. Gravity measurements at sea by use of the T.S.S.G. Part 2. Results of the measurements. J. Phys. Earth, **18**, 203-284.

Seno, T. and G.C. Kroeger, 1983. A reexamination of earthquakes previously thought to have occurred within the slab between the trench axis and double seismic zone, northern Honshu arc. J. Phys. Earth, **31**, 195-216.

Stauder, W., 1968. Tensional character of earthquake foci beneath the Aleutian trench with relation to sea-floor spreading. J. Geophys. Res., **73**, 7693-7701.

Suzuki, S., Y. Motoya, N. Umino, A. Hasegawa, S. Kameya, and K. Tanaka, 1983. Hypocentral distribution and composite focal mechanisms of shallow earthquakes near the junction between the Kurile and the northeastern Japan arcs. Zisin, **36**, 407-421 (in Japanese).

Takagi, A., A. Hasegawa and N. Umino, 1977. Seismic activity in the northeastern Japan arc. J. Phys. Earth, **25**, s95-s104.

Takanami, T., 1982. Three dimensional seismic structure of the crust and upper mantle beneath the orogenic belts in southern Hokkaido, Japan. J. Phys. Earth, **30**, 87-104.

Takeo, M., M. Kasahara and K. Abe, 1982. Source process of the 1982 Urakawa-Oki earthquake. Abst. Ann. Meet. Seismol. Soc. Japan, No. 2, A02 (in Japanese).

Umino, N. and A. Hasegawa, 1975. On the two-layered structure of a deep seismic plane in the northeastern Japan arc. Zisin, **28**, 125-139 (in Japanese).

Yoshii, T., 1979 a. A detailed cross-section of the deep seismic zone beneath northeastern Honshu, Japan. Tectonophysics, **55**, 349-360.

Yoshii, T., 1979 b. Compilation of geophysical data around the Japanese islands (I). Bull. Earthq. Res. Inst., **54**, 75-117 (in Japanese).

Wallace, T.C., D.V. Helmberger, and G.R. Mellman, 1981. A technique for the inversion of regional data in source parameter studies. J. Geophys. Res., **88**, 1679-1685.